JMEPEG (2022) 31:3688–3703
https://doi.org/10.1007/s11665-021-06507-4

©ASM International
1059-9495/$19.00

TECHNICAL ARTICLE

Investigation of the Structural and Tribological Properties of 316L Stainless Steel Manufactured Using Variable Production Parameters by Selective Laser Melting

Ufuk Gençoğlu, Gürkan Kaya, T. Oğuzhan Ergüder, İlyas Hacısalihoğlu, and Fatih Yıldız

Submitted: 10 October 2021 / Revised: 18 November 2021 / Accepted: 2 December 2021 / Published online: 20 January 2022

The structural, tribological and mechanical properties of the engineering parts manufactured by the selective laser melting (SLM) method are highly affected by the strategies and parameters used in manufacturing. Therefore, it is extremely important to know/control the effect of the parameters to be used in manufacturing on the mechanical and tribological properties of the material and to determine the optimum production conditions. In this study, the effects of these fabrication parameters of SLM process on the structural, mechanical properties and wear performance of 316L stainless steel were investigated. Because many production parameters are involved in the SLM method, it was tried to save material and time by systematically reducing the manufacturing parameters. In experimental studies, the parameters of scanning speed, laser beam power and hatch spacing, which directly affect the laser energy density, were investigated. As a result, it was determined that the manufacturing parameters/strategies used in the SLM method have a significant effect on the mechanical properties and wear performance of 316L stainless steel. The lowest wear rate was obtained for the sample produced with 70% hatch spacing and 0° build orientation. This sample also represented the parameter in which the highest microhardness and density ratio was obtained.

Keywords additive manufacturing, laser parameters, mechanical properties, selective laser melting, wear, 316L stainless steel

1. Introduction

Because of its ductility, biocompatibility and high corrosion resistance, stainless steels are widely used materials in many areas as biomedical, construction, aerospace and automotive industry (Ref 1-5). 316L stainless steel is the most widely used type of stainless steel. Due to its superior properties, 316L stainless steel is widely used in the production of parts with functional and complex geometries in additive manufacturing (Ref 6. The selective laser melting (SLM) method, which is one of the additive manufacturing methods, is a new generation production technology in which products with complicated geometries can be manufactured (Ref 7). The parts manufactured by the SLM method are significantly affected by the production parameters and strategies in terms of structural, mechanical and tribological properties. Literature studies on the characterization of 316L stainless steel material produced by SLM method were discussed in this section.

In a study by Morgan et al., the effects of Q switch pulsing frequency, scanning speed and scan spacing on the density were investigated on samples produced using 316L stainless steel powder. It was concluded that material density is related to energy density (Ref 8). Li et al. examined the effect of production parameters on the tribological performance of 316L stainless steel sample manufactured with SLM. Prismatic samples were manufactured at different build orientations and laser beam powers using the SLM method, and wear tests were carried out. In the samples produced with low laser beam powers, lower hardness was formed, and density and lack of fusion were observed at the melt pool boundaries. But, it was concluded that the effects of build orientation and laser beam power on the wear rate and coefficient of friction were not notable (Ref 9). Sun et al. investigated the wear behavior of 316L stainless steel manufactured by the SLM method and its corrosion properties in a chloride containing solution. They determined that 316L stainless steel manufactured with the SLM method exhibited worse wear resistance compared to standard cast 316L stainless steel. They concluded that the wear rate of the stainless steel produced with SLM is due to the amount of porosity in the structure (Ref 10). Li et al. studied the effects of different test conditions and build directions on the tribological behavior of 316L stainless steel samples manufactured with SLM. They determined that the build orientation did not have a significant effect on the wear rate and coefficient of friction. They concluded that the coefficient of friction decreased and material loss reduced at temperatures above 200°C because the oxide films acted as lubricants (Ref 11). Huang et al. investigated the relationship between wear performance and microstructure of selective laser melted 316L stainless steel. They found that the wear performance of 316L stainless steel produced with SLM was better than the wear performance of rolled samples and also observed that the

Ufuk Gençoğlu, Gürkan Kaya, T. Oğuzhan Ergüder, İlyas Hacısalihoğlu, and **Fatih Yıldız**, Department of Mechanical Engineering, Erzurum Technical University, 25050 Erzurum, Turkey. Contact e-mail: fatih.yildiz@erzurum.edu.tr.

normal load applied in the wear test had little effect on the coefficient of friction (Ref 12). Bartolomeu et al. analyzed the effect of three different manufacturing technologies (SLM, traditional casting and hot pressing) on the mechanical, microstructure properties and wear behavior of 316L stainless steel. They concluded that the mechanical properties and tribological performances of 316L stainless steel samples produced with SLM were higher compared to traditional casting and hot pressing. They stated that the high mechanical and wear performance of 316L stainless steel manufactured with SLM was mainly due to its fine-grained microstructure (Ref 13). Zhu et al. examined the wear and friction behavior of 316L stainless steel manufactured by both SLM and traditional methods under lubricated conditions. They observed that the sample produced with SLM had lower wear and friction than the traditionally manufactured sample. It was stated that the tribological performance of the parts produced by the SLM method could be better than the samples manufactured with traditional method due to the fine grains in the microstructure if the pores can be greatly reduced (Ref 6). Yusuf et al. analyzed the tribological behavior of the material by applying high-pressure torsion—HPT, to 316L stainless steel samples manufactured with the SLM method. They observed that the wear performance increased with the ultra-fine grain structure obtained after the HPT process. The fine-grained structure resulted in high hardness, and therefore, an improvement in overall wear resistance was considered (Ref 14).

According to the literature review, it has been determined that studies on the production of 316L stainless steel material using the SLM method usually focus on microstructural and mechanical studies, and studies evaluating tribological properties are quite limited. In addition, it has been observed that the scanning speed, layer thickness, hatch spacing and laser beam power values are kept constant for a one energy density in the production processes performed with the SLM method, and the effects of these parameters on the microstructural, mechanical and tribological properties were not demonstrated systematically. It has been determined that the effects of the hatch spacing and build orientation parameters on the wear performance of 316L stainless steel are not considered as a whole, especially in the productions made with the SLM method. Therefore, the effects of SLM production parameters on the mechanical, tribological and structural properties of 316L stainless steel were investigated and the obtained results were compared with the properties of the traditionally produced stainless steel in this study.

2. Experimental Details

In this study, austenitic 316L stainless steel powder material was used in the production processes with the SLM method, and its chemical composition is given in Table 1. In order to compare the structural, mechanical and tribological analyses, 316L stainless steel material produced by the traditional method (forging) was used. Powder size and distribution of 316L stainless steel powder were examined by taking SEM images (Fig. 1). For 316L stainless steel powder material, the powder size was determined as 10-45 μm. When the SEM image was examined, it was seen that the powder used was quite spherical and did not exhibit flocculence behavior.

Table 1 Chemical composition of 316L stainless steel powder material

Element	wt.%
C	0–0.030
S	0–0.030
Si	0–1.0
Mo	2.0–2.5
Mn	0–2.0
P	0–0.045
Cr	16.5–18.5
Ni	10.0–13.0
Fe	Balance

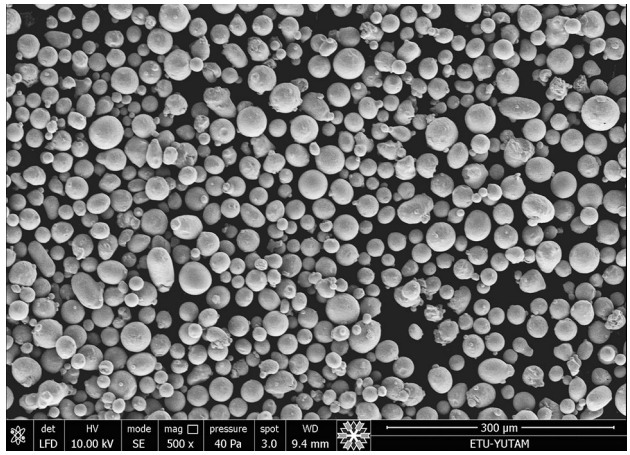

Fig. 1 The morphological image of as-received 316L stainless steel powders

Test samples used for structural, mechanical and tribological examinations were produced with Concept Laser M LabR SLM device (max. 100 W) using different production parameters. Productions with SLM were carried out in an atmosphere of nitrogen (N_2) gas using the continuous laser pulse mode. Oxygen content was kept below 1% during production. STL file formats of the produced test samples were prepared with the help of AutoFab software. In order to investigate the molten pool formed in different parameters, single laser pulses with a powder layer thickness of 25 μm were made on a 316L stainless steel plate. These laser pulses were applied in the range of laser scanning speed (from 200 to 2000 mm/s in 200 increments) and laser beam power (from 20 to 100 W in 20 increments). In order to examine the cross-sectional images, the plate was cut in the middle to be perpendicular to the laser traces. Afterward, the samples were sanded using water sandpaper numbered 240, 400, 600, 800 and 1200, respectively, and polished with diamond suspension. The cross-sectional images were taken with the Zeiss Axio A1 optical microscope, the depth (B) and width (A) of the melt pools obtained were examined, and the aspect ratios ($R = A/2B$) were calculated. In order to investigate the effect of hatch spacing on mechanical properties, tensile samples at different hatch spacing values were produced by choosing the parameters with the best R ratio determined. The hatch spacing can be defined as the separation between two consecutive laser beams. The produced tensile samples were sized according to the ASTM E8 standard. The

macroimage of tensile samples on the SLM platform is shown in Fig. 2. As a result of the tensile tests, 10x10x5 mm prismatic wear test samples were produced from the parameters with the best mechanical properties.

The phases on the samples manufactured with SLM method were detected by the GNR-Explorer XRD device using Cu-Kα radiation with a wavelength of λ = 1.5405 A°. Measurements were obtained at 0.05° steps per second with a symmetrical scan configuration in the 20°-80° range. The obtained peak cards were examined with Match software and compared with the results in the literature.

The surface morphologies of the single laser traces and the melt pool on the stainless steel plate were investigated using the Carl Zeiss Scope A1 optical microscope device. In order to investigate the surface morphologies of the single laser traces and the melt pool, Glyceregia (10 ml HNO_3, 20-50 ml HCl, 30 ml glycerol) solution was prepared and etched. In addition, the etched surface images of the contour and test samples manufactured with SLM method were investigated with an optical microscope.

Wear tests were carried out with Bruker-UMT tribometer tester device. The test parameters of the wear tests are given in Table 2 and three measurements were taken for each parameter.

QUANTA – FEG 250 scanning electron microscope (SEM) was used for morphological analysis of the 316L stainless steel powder material, wear traces, characterization of the contour structures, fracture surface images of the tensile samples and microstructure images of the prismatic samples. Bruker Contour GT 3D profilometer device was used to examine the surface roughness values of the samples and to calculate the wear volumes after the wear tests. The wear volumes were obtained by multiplying the cross-sectional area of the wear trace, which was determined by taking a mean of ten measurements from each wear trace, by the length of wear trace. SHIMADZU HMV-G20 microhardness device was used for microhardness measurements. The measurements were taken with the Vickers method by taking at minimum ten measurements from different parts of the sample surfaces with a dwell time of 10 s under 100 g load. Tensile tests of cylindrical tensile samples produced by the SLM method and sized as to ASTM E8 standard were performed in INSTRON 5982 static test device. All samples were tested at room temperature conditions and with a tensile velocity of 1 mm/min.



Fig. 2 Macroimage of tensile samples on the SLM platform

3. Results and Discussion

3.1 Determination of SLM Production Parameters

3.1.1 Surface Morphology of Single Laser Traces. In order to determine the homogeneity of the laser traces resulting from the interaction of laser beam power and scanning speed used in the production, the powder layer thickness was kept constant at 25 μm during the production process. Single laser traces were applied on 316L stainless steel plate with five different laser beam powers and ten different laser scanning speeds at 25 μm layer thickness. Optical microscope morphology images of the surfaces obtained as a result of single laser pulses are presented in Fig. 3. It was determined that both laser scanning speed and laser beam power values have a significant effect on the formation of single laser traces. Due to insufficient melting caused by low laser beam power and high scanning speeds, no traces of melting were observed in the 316L stainless steel plate as a result of laser pulses performed at a laser beam power of 20 W and a laser scanning speed range of 1200-2000 mm/s (A region). Single laser traces formed in the B region have very low width and depth because of insufficient melting. Although continuous traces were observed in the C region, it was observed that there were instabilities in the melt region and a continuous melting line could not be formed. It was determined that the single laser traces formed in the D region with high laser beam powers were continuous and more stable.

3.1.2 Melt Pool Morphology. The cross-sectional images taken from the traces formed after single laser pulses on the 316L stainless steel plate are given in Fig. 4. With the help of the images given in Fig. 4, the width and depth of the melt pools formed after the SLM process were examined. As a result of insufficient melting caused by low laser beam power, after single laser pulses performed with 20 W laser beam power, no melting could be obtained in the stainless steel plate at all scanning speed values and the sizes of the melt pool could not be determined. Although the depth was very low, the melt pool became apparent at 40 W laser beam power and scanning speeds of 600 mm/s and below. Due to increasing laser beam power and decreasing laser scanning speed values, the melt pools were obtained more distinctly because the energy density and the amount of energy absorbed by the powder bed increased. When the optical microscope images of the melt pools were examined, two different pool shapes occurred in the form of a keyhole and an ellipse. The dimensional properties of the melt pool obtained with different laser beam power and

Table 2 Wear test parameters

Test parameters	Values
Test type	Reciprocating
Ambient	Dry conditions
Temperature (°C)	Room temperature (23 ± 2)
Ball type	Al_2O_3
Time (s)	3600
Normal load (N)	3
Velocity (mm/s)	8
Stroke (mm)	4

laser scanning speeds and the aspect ratio (R) values representing the melt pool form are presented in Table 3. $R \geq 1$ values represented the conductive mode in which the melt pool was elliptical, while $R < 1$ values represent the keyhole mode. The keyhole form usually occurred in production conditions where laser beam powers were high and scanning speed values were low. When the molten pool form changed from the keyhole mode to the conductive mode, the molten pool geometry changed from V shape to ellipse shape. In many studies in the literature, it was been reported that porous structures appeared after the overlap of the melt pools in the later stages of production in keyhole mode melt pools (Ref 15). In a study examining the melt pool form, the melt pool with conductive mode was preferred because it created a non-porous structure as a result of more balanced thermal distribution in the melt pool (Ref 16). Considering the aspect ratio (R) values given in Table 3, it was determined that 600, 800 and 1000 mm/s scanning speed parameters provided the optimum melt pool forms at 100 W laser beam power with conductive mode and aspect ratio approaching to 1.

3.1.3 Characterization of Contour Structures Produced by SLM Method and Optimization of Laser Scanning Speed. Contour productions were carried out using 600-800-1000 mm/s laser scanning speed and 100-W laser beam power values, which were the optimum laser production parameters determined after the melt pool form examinations. The appearance of the contour structures produced in 4x5x6 mm dimensions is given in Fig. 5. SEM images of the produced contour structures are given in Fig. 6, and the optimum scanning speed value was determined by examining the images.

When the SEM images of the contour structures were investigated, it was observed that the contour walls were not homogeneous and thinning occurred in some parts of the trace in the productions performed at 800 and 1000 mm/s scanning speeds. In the productions carried out with a laser scanning speed of 600 mm/s, it was determined that the contour wall was quite homogeneous unlike the structures obtained with the other two scanning speeds. According to these examinations, the production parameters for the 25 μm layer thickness were determined as 600 mm/s scanning speed and 100 W laser beam power.

3.1.4 Optimization of Hatch Spacing Parameter for Manufacturing Processes with SLM Method. In this study, in which SLM production parameters were optimized by systematically reducing the parameters, the optimum hatch spacing value was tried to be determined after the laser scanning speed and laser beam power values were determined. In order to determine the hatch spacing values, metallographic polishing process was applied to the contour structure produced with 600 mm/s laser scanning speed and 100 W laser beam power determined in the previous stage. The thickness of the contour wall was measured via optical microscope as a basis for hatch spacing (Ref 17). The optical microscope image of the contour structure is given in Fig. 7. According to the measurement taken on the contour structure, the wall thickness was determined as 100 μm.

According to the determined wall thickness value, the amount of hatch spacing was examined in the range of 30-90 μm, with 10% increments when it ranged from 30 to 90%, and tensile samples were produced perpendicular to the build platform by using these hatch spacing values. Three tensile samples were produced for each hatch spacing value and tensile tests were performed. The tensile curves obtained for varying values of hatch spacing are given in Fig. 8.

When the mechanical properties of 316L stainless steel manufactured by the traditional method (forging) were examined in the literature, it was reported that the tensile stress was 500 MPa and the elongation at break was approximately 65% (Ref 18). The most basic deficiency in the SLM process, one of the additive manufacturing methods, is insufficient elongation values resulting from insufficient joining and high cooling rate (Ref 19). For this reason, the elongation value at fracture was taken as the basis of the performance criterion in terms of mechanical properties. When the tensile curves obtained for different hatch spacing values were examined, the lowest elongation values were obtained as 52% and 58% for the samples produced with 30% and 40% hatch spacing values, respectively. The graph showing the change in elongation values for different hatch spacing values is presented in Fig. 9. The highest elongation values were obtained for 60%, 70% and 80% hatch spacing values, and the elongation values started to decrease as a result of insufficient joining after 90% hatch spacing. There was no notable difference between the samples in terms of tensile stresses, and values in the range of about 500-550 MPa were obtained. In Fig. 9, where the tensile graphs for different amounts of hatch spacing were given comparatively, 60%, 70% and 80% hatch spacing values, in which the highest elongation values were acquired, were determined as the optimum value range at this stage.

The fracture surface SEM images of the tensile samples produced by the SLM method using 600 mm/s laser scanning speed, 100 W laser beam power and different hatch spacing values are given in Fig. 10. When the SEM images were examined, it was pointed out the pores arising from the production with SLM in the 30-50% hatch spacing. It was determined that these pores were significantly reduced in the 60-80% hatch spacing range, and pores reappeared for the 90% hatch spacing value.

3.1.5 Microstructural Properties, XRD Results and Density Measurements. Prismatic test samples were produced by the SLM method using three different build orientations (0°, 45° and 90°) for optimum hatch spacing values (60-70-80%) determined after mechanical examinations. Microstructure SEM images taken from the surfaces of these samples are given in Fig. 11. Fine cellular/dendritic structure was seen in the microstructure images (Ref 20). This microstructure was formed as a result of rapid solidification due to the high cooling rates encountered in the SLM method, as in the structures obtained by the casting technique (Ref 21). It was observed that the cellular microstructure was dominant in the samples produced with 0° build orientation but some grains grew as dendritic and the microstructure was more homogeneous. It was also determined that with the increase in the build orientation (45° $\rightarrow$ 90°), the grains were preferentially oriented (epitaxial growth) in the microstructure and the dendritic growth

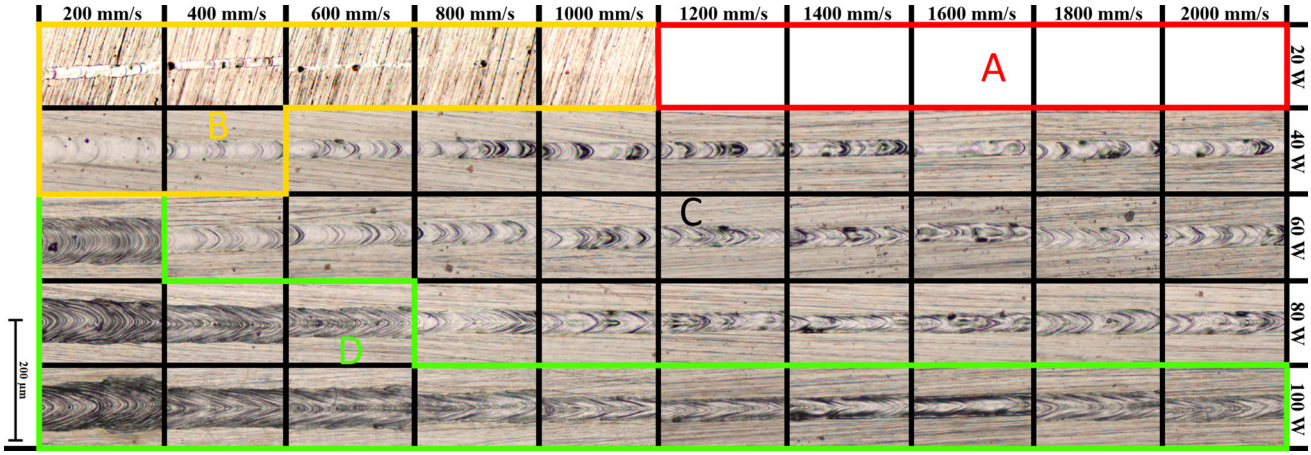

Fig. 3. Surface morphology images of single laser pulses performed at different laser beam powers and laser scanning speeds

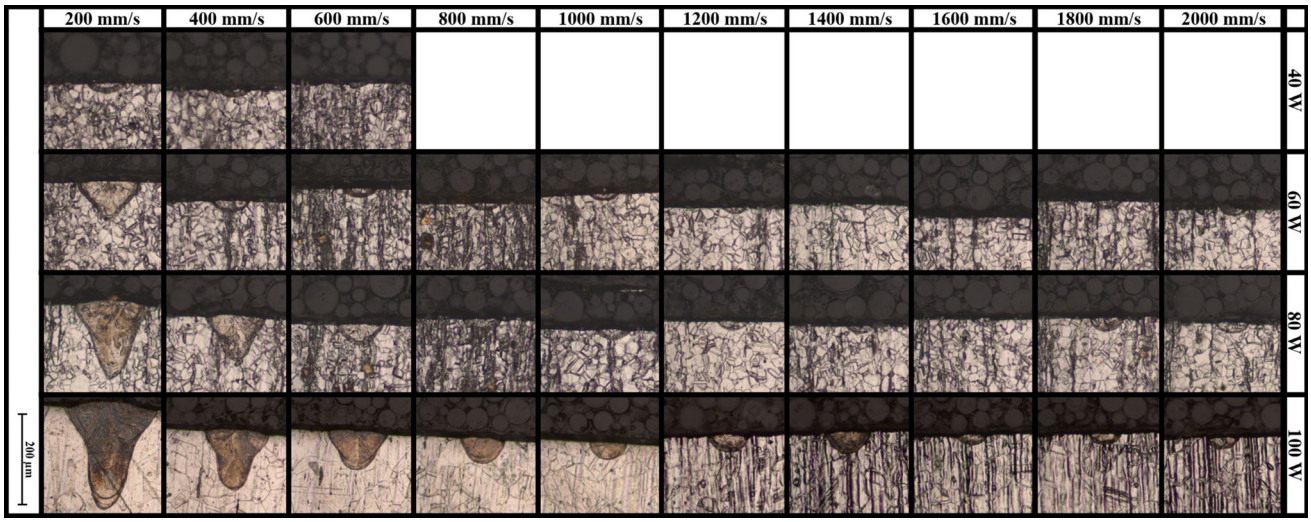

Fig. 4 Melt pool images of single laser pulses performed at different laser beam powers and laser scanning speeds

intensified (Ref 22-24).

The XRD results of 316L stainless steel produced using the traditional method and the SLM method using different hatch spacing values and build orientations are given in Fig. 12. In all samples, γ-Fe peaks with FCC structure were obtained for (111), (200) and (220) planes (Ref 20). Despite the very high cooling rate during the SLM process, only the austenite phase was obtained due to the presence of the austenite-forming element Ni (Ref 24). When the peaks of the samples produced at different hatch spacing values using the 0° build orientation were examined, it was observed that the intensity values were very close to the traditional sample in all three planes. For the samples produced in 45° and 90° build orientations, they were determined that the peaks expanded and their intensity increased especially in the (200) plane. This situation indicates the presence of residual stresses and high strain (Ref 20, 25). In the overall evaluation made according to the XRD results, it was determined that the build orientation on the crystal structure has a greater effect than the hatch spacing parameter.

The density ratio of the samples produced at three different hatch spacing values (60-70 and 80%) for 0° build orientation by SLM method was measured with the help of helium pycnometer, and the value of hatch spacing with the highest density ratio was determined. The obtained density values are given in Table 4. The density of 316L stainless steel produced by traditional methods is 8.0 g/cm^3, and the density values in production with SLM were obtained a little lower as expected. The density value of the sample produced with 70% hatch spacing was 7.8914 g/cm^3, and it was determined as the production parameter with the highest density ratio. In a study using different production parameters, the average density of 316L stainless steel produced with SLM was obtained as 7.821 ± 0.005 g/cm^3 (Ref 20).

Table 3 Dimensional properties of the melt pool obtained with different laser beam powers and different scanning speeds

Laser beam power, W	Scanning speed, mm/s	Width-A, μm	Depth-B, μm	Ratio-R, $R = A/2B$
40	200	83.199	21.841	1.905
	400	66.106	15.815	2.090
	600	45.629	9.054	2.520
	800			
	1000			
	1200			
	1400			
	1600			
	1800			
	2000			
60	200	136.541	85.006	0.803
	400	81.616	24.248	1.683
	600	72.365	18.497	1.956
	800	66.986	15.507	2.160
	1000	63.969	13.771	2.323
	1200	51.959	14.147	1.836
	1400	53.613	12.811	2.092
	1600	44.924	11.534	1.947
	1800	62.913	17.856	1.762
	2000	59.846	14.798	2.022
80	200	155.200	154.700	0.502
	400	128.600	82.200	0.782
	600	100.900	39.200	1.287
	800	83.100	26.090	1.593
	1000	72.140	19.850	1.817
	1200	61.560	18.200	1.691
	1400	59.560	15.350	1.940
	1600	62.260	17.580	1.771
	1800	76.856	22.784	1.687
	2000	70.728	22.143	1.597
100	200	208.600	230.530	0.452
	400	139.600	126.270	0.553
	600	128.700	76.800	0.838
	800	97.800	52.400	0.933
	1000	79.700	36.700	1.086
	1200	87.400	33.600	1.301
	1400	97.600	42.000	1.162
	1600	64.600	19.100	1.691
	1800	69.200	22.200	1.559
	2000	66.200	23.300	1.421

3.2 Characterization of Tribological Properties

Wear tests were performed on samples produced using three different build orientations on the SLM platform, shown schematically in Fig. 13. In addition, 60%, 70% and 80% hatch spacing values were used for each build orientation, and the test surfaces of the samples were indicated on the figure. In addition to the wear tests, microhardness measurements were also applied to the sample test surfaces shown in Fig. 13.

The friction coefficient (COF) results of the samples manufactured with the SLM method and the traditional 316L stainless steel are given in Table 5. The surfaces of both the SLM samples and the traditional sample were polished using metallographic methods before performing the wear test. The surface roughness values of the samples were prepared to be approximately 0.15 μm. The average COF of 316L stainless steel produced by the traditional method was determined as approximately 0.75, and the result was obtained in accordance

with the studies in the literature (Ref 26). It was determined that the COF values obtained for all samples manufactured with the SLM method were lower than the sample produced by the traditional method. The lowest COF values were obtained for samples produced with 60-70% hatch spacing values and 0° build orientation.

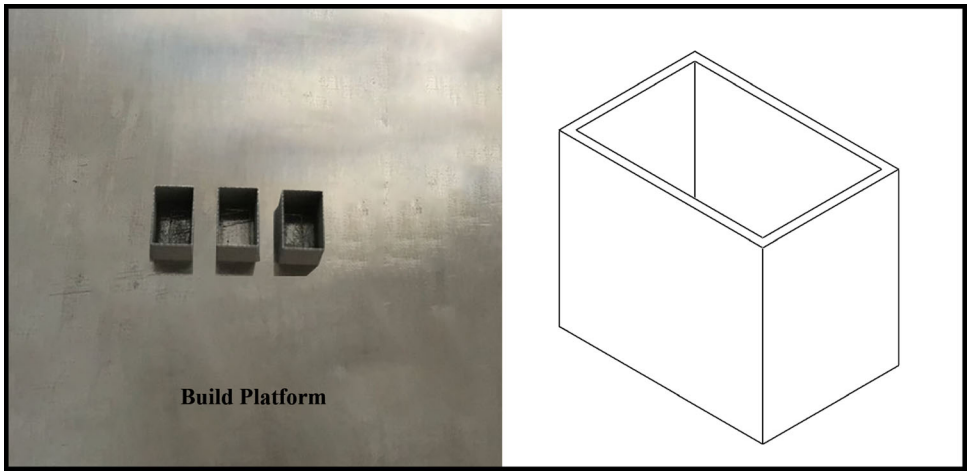

Fig. 5 The geometry of the contour structures and their appearance on the build platform

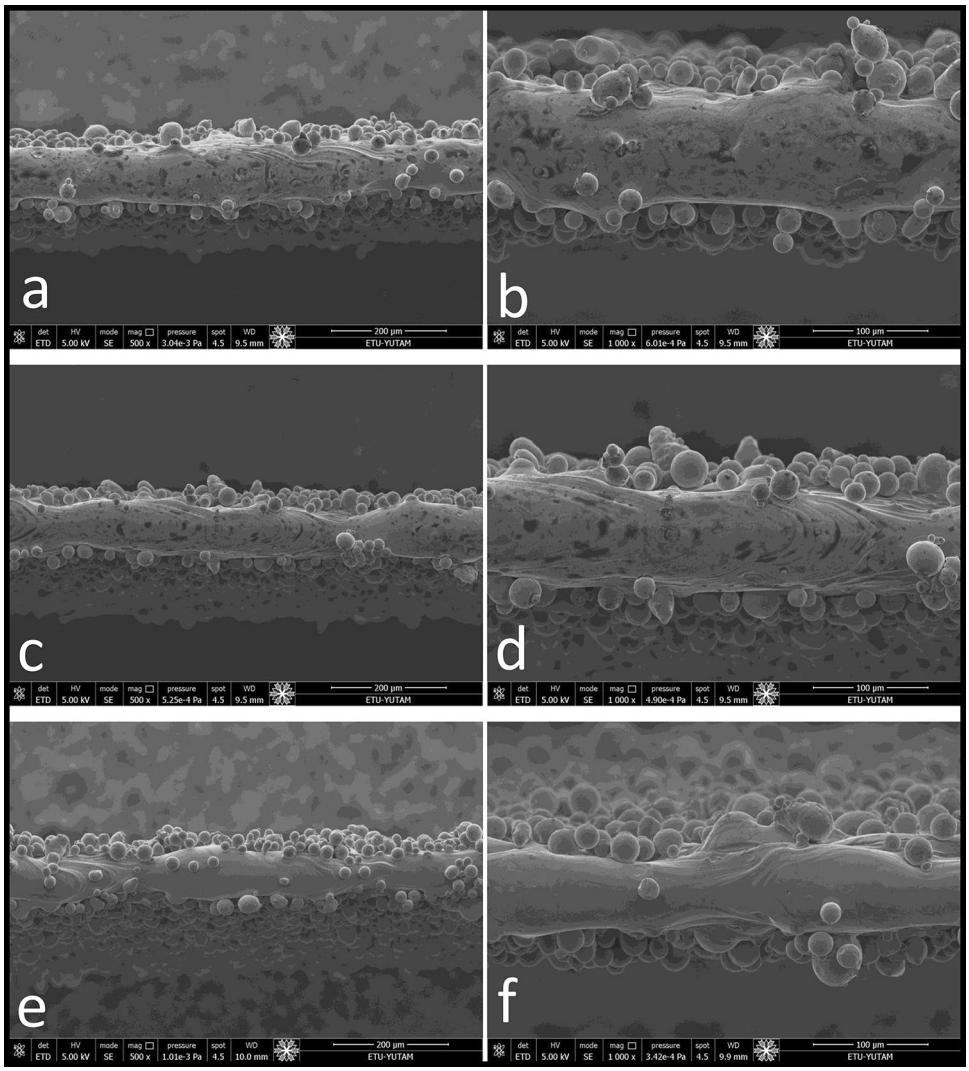

Fig. 6 SEM images of contour structures, (a-b) 100 W-600 mm/s, (c-d) 100 W-800 mm/s, (e-f) 100 W-1000 mm/s

The graph showing the microhardness and wear rate values of the samples manufactured with the SLM method using different parameters and the sample manufactured with the traditional method is presented in Fig. 14. The microhardness value of the stainless steel manufactured by the traditional method was measured as approximately 155 $HV_{0.1}$. The microhardness values of the samples produced by the SLM method increased as a result of the changing microstructure with the effect of rapid cooling. This change in microhardness values was more pronounced especially for the samples produced with 0° build orientation at all three hatch spacing values. The highest microhardness value was measured as 205 $HV_{0.1}$ for the sample produced with 70% hatch spacing and 0° build orientation, and an increase of approximately 20% was obtained compared to the traditional sample.

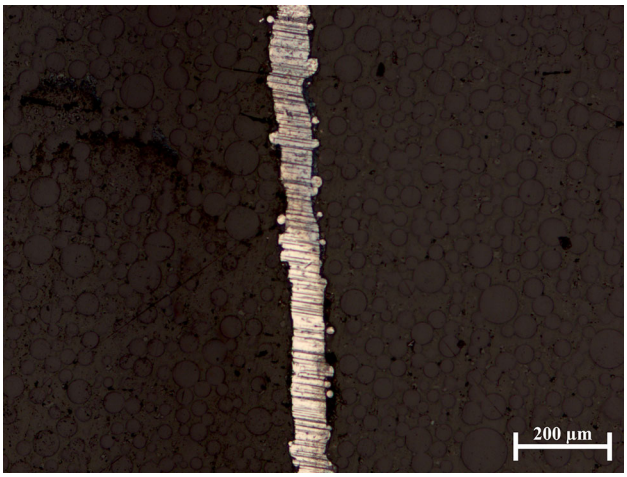

Fig. 7 Optical microscope image of the contour structure produced with the parameter 100 W-600 mm/s

According to the wear rate values given in Fig. 14, it was observed that the wear rate increased due to the increase in the build orientation within all three hatch spacing values in the samples manufactured with the SLM method. The lowest wear rate was obtained for the sample (70-0°) produced with 70% hatch spacing and 0° build orientation. This sample also represented the parameter in which the highest microhardness and density ratio was obtained. The wear rate value of the 70-0° sample was obtained as 17% lower than the wear rate of the sample manufactured by the traditional method. It was determined that 60% and 80% of the hatch spacing values exhibited higher wear rate values compared to 70% in the samples produced with 0° build orientation, where lower wear rates were obtained compared to the traditional sample.

It was clearly seen that the thermal accumulation in the sample produced with 60% hatch spacing was higher than the other values. Accordingly, the high energy transferred to the structure had a negative effect on the microstructure. It was known that the overlap distance in the laser traces decreased at the 80% hatch spacing value. It was determined that this situation caused an increase in the amount of voids and pores in the structure and therefore an increase in wear rates. In SLM production processes using variable build orientations, the number of layers increased with increasing build orientation angles. For that reason, the cooling conditions of the solidified layers changed. It was determined that the number of layers of SLM samples produced with 45° and 90° build orientations is higher than the sample produced with 0° build orientation. The increase in the number of layers caused a decrease in the microhardness values and an increase in the wear rate values. As a result, 70% hatch spacing value was determined as the optimum value in terms of microhardness and wear rate values. It was not necessary to carry out wear tests for the samples produced with lower and upper hatch spacing values such as 50% and 90%, since the downward trend in terms of wear rate started at the hatch spacing values below and above these values (60% and 80%).

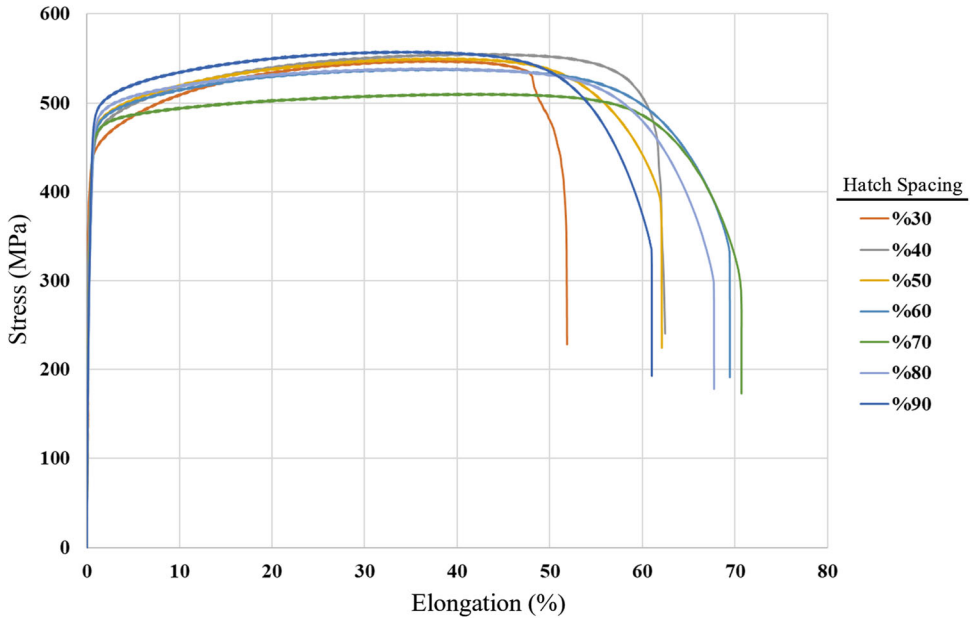

Fig. 8 Tensile curves of samples produced with different hatch spacing

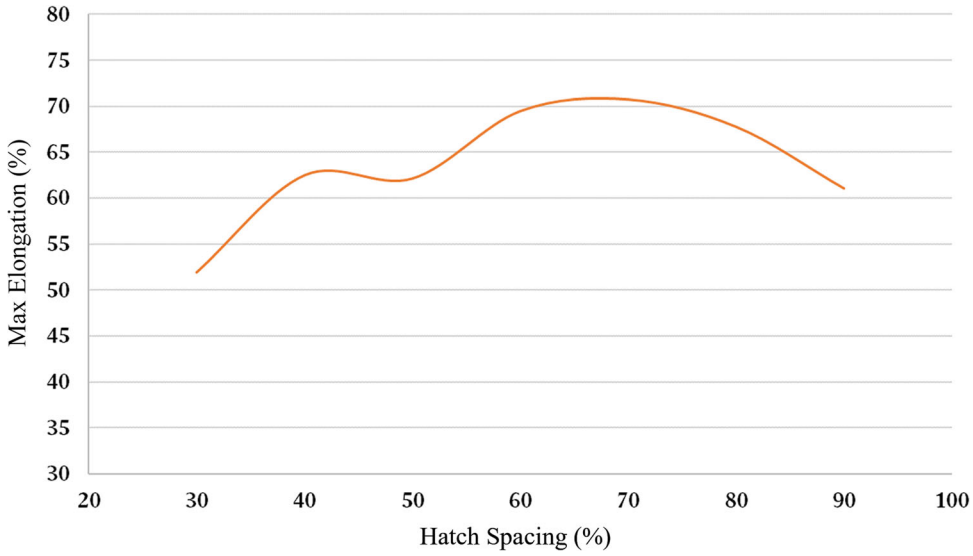

Fig. 9 The change in the elongation values of the samples produced with various hatch spacing values

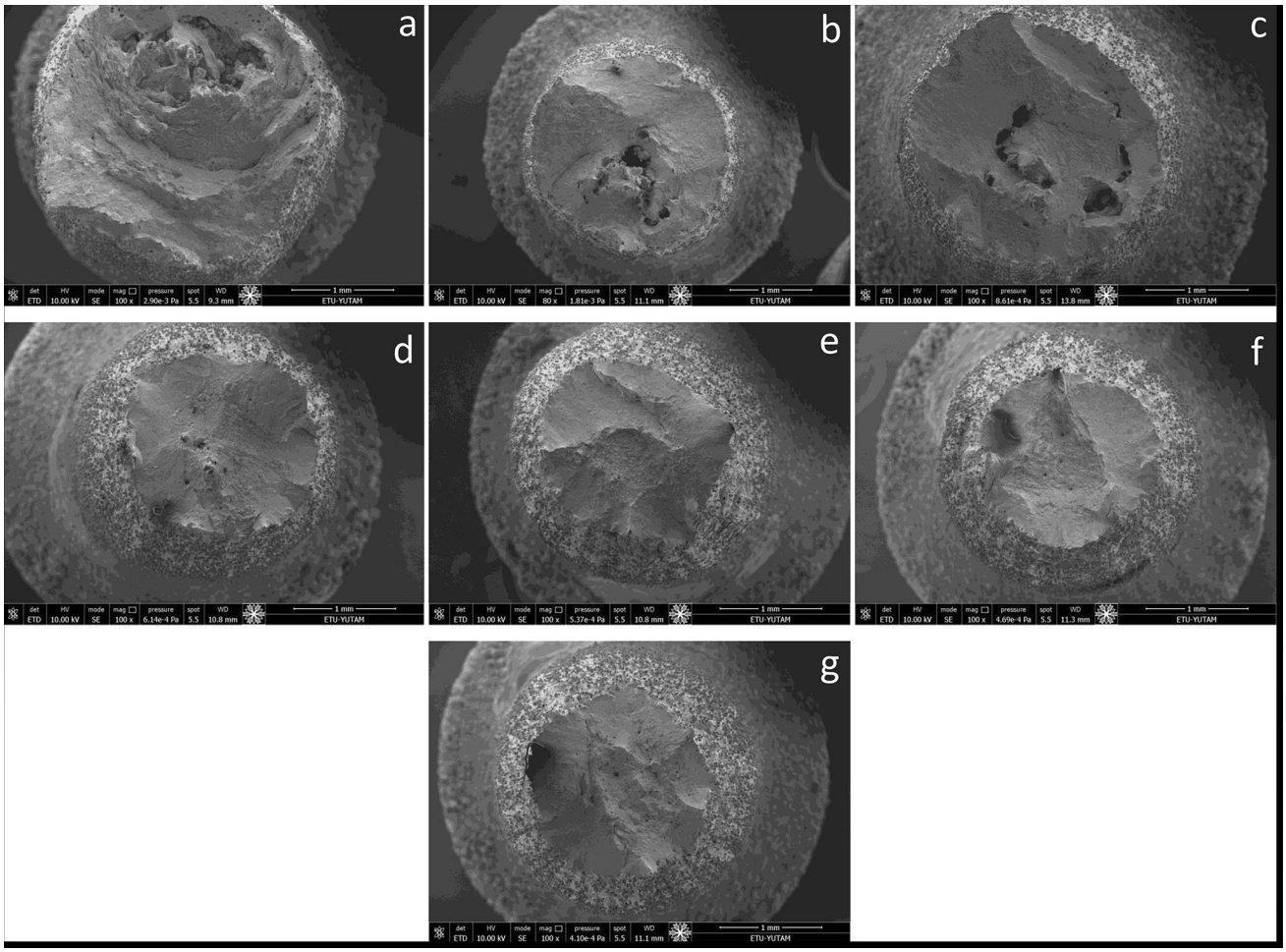

Fig. 10 Fracture surface SEM picture of tensile samples produced with various amounts of hatch spacing, (a) %30 hatch spacing, (b) %40 hatch spacing, (c) %50 hatch spacing, (d) %60 hatch spacing, (e) %70 hatch spacing, (f) %80 hatch spacing, (g) %90 hatch spacing

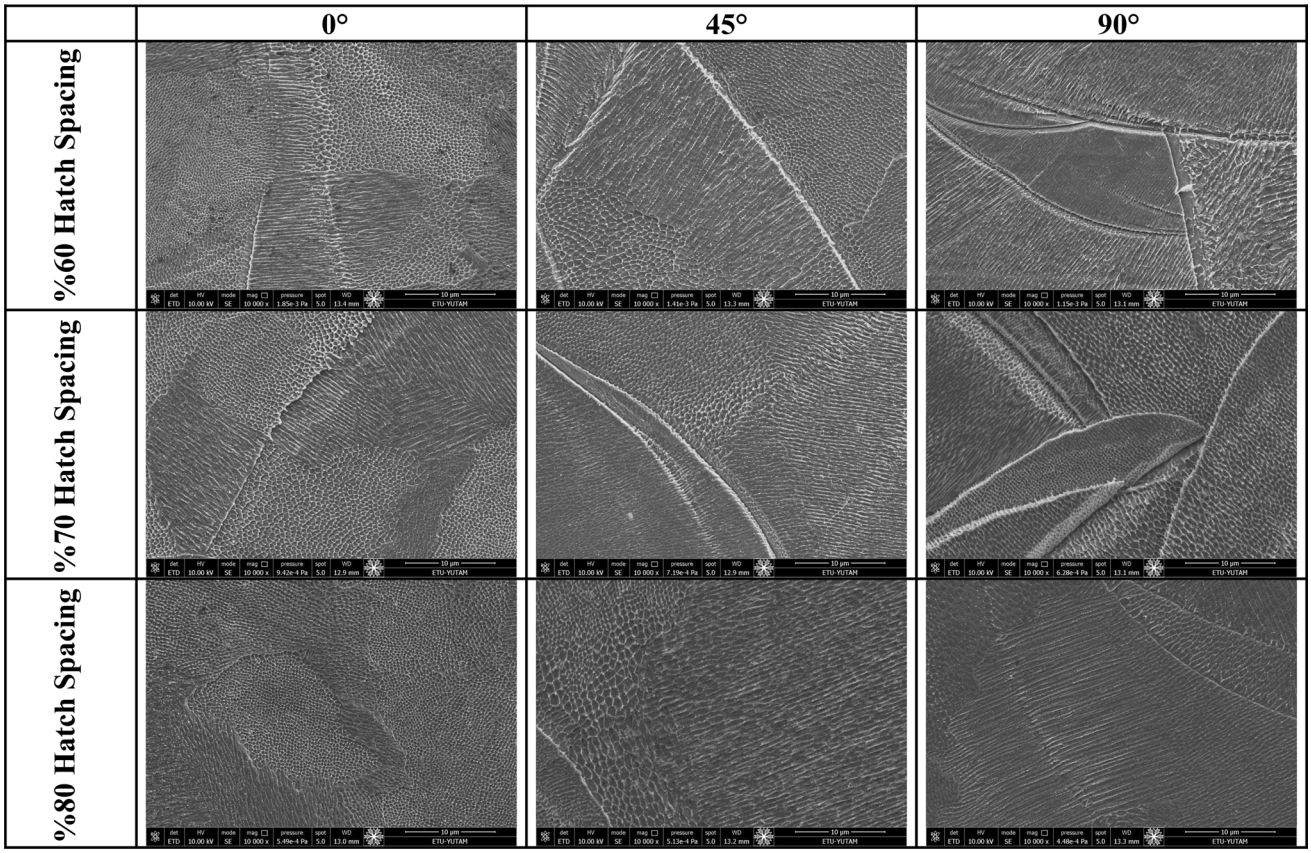

Fig. 11 Microstructure SEM images of samples produced at different hatch spacing values and build orientations

Wear trace SEM images and 3D optical profilometer images of 316L stainless steel material produced by using different hatch spacing values and build orientations by the SLM method and traditional method are given in Fig. 15-17. The images of the samples produced in different build orientations for each hatch spacing value were presented, combined with the images of the traditional sample as reference. When the SEM images of the worn surfaces were examined, it was determined that the wear mechanism for the stainless steel material produced by both traditional and SLM methods was a combination of adhesive wear, abrasive wear and plastic deformation mechanisms. The adhesion formed by the contact of the stainless steel material and the counter-abrasive (Al_2O_3) pin material caused the formation of wear debris in the later stages of the wear test. Wearing pairs and the wear products formed between these pairs caused three-body wear, increasing the amount of wear and causing the abrasive wear mechanism. The formation of abrasive channels formed after this effect was clearly seen in all samples. In addition, the piles up at the edges of the wear trace clearly indicated the plastic deformation that occurred during the test. As a general evaluation, the wear trace width of traditional 316L stainless steel was obtained higher than the samples produced with the SLM method. In all samples produced by the SLM method, the wear trace widths increased due to the increase in the build orientation. The lowest wear trace width was obtained in the 70-0° sample, which had the highest surface hardness and lowest wear rate values. Considering all the hatch spacing values and the surfaces on which the wear tests were carried out (Fig. 13), the 0° build orientation was determined as the most suitable orientation in terms of wear resistance.

4. Conclusions

In this study, the structural, mechanical and tribological properties of 316L stainless steel material produced by the SLM method and the traditional forging method were investigated comparatively. Since there are many production param-

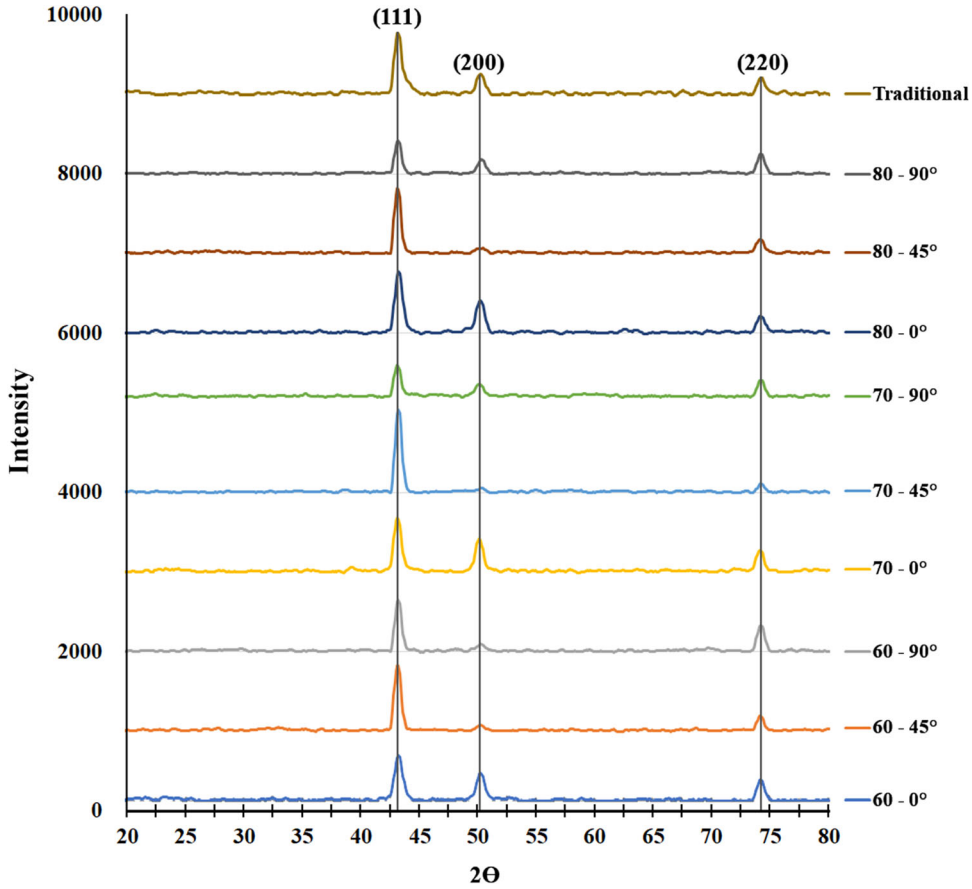

Fig. 12 XRD graph of samples produced at different hatch spacing values and build orientations

Table 4 Density and density ratio values of the samples produced with 60%, 70% and 80% hatch spacing values

Hatch spacing value (%)	Density (g/cm^3)	Density ratio (%)
60	7.7617	97.02
70	7.8914	98.64
80	7.8768	98.46

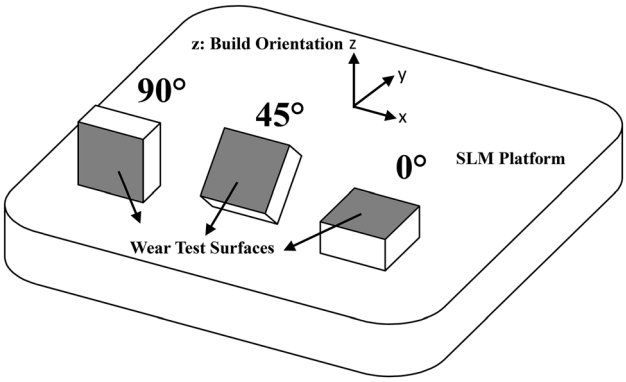

Fig. 13 Schematic representation of wear test samples produced by SLM method in different build orientations

Table 5 The average COF values of the samples manufactured by the SLM method using different parameters

Samples	The average COF values
Traditional	0.7511
60-0°	0.5551
60-45°	0.6972
60-90°	0.5563
70-0°	0.5650
70-45°	0.5619
70-90°	0.6975
80-0°	0.7108
80-45°	0.6981
80-90°	0.7065

eters in the production processes carried out with the SLM method, parameter reduction was made systematically while determining the optimum production parameters. Thus, material and time savings were achieved. The results obtained after the study were summarized below:

- After single laser pulses on 316L stainless steel plate, both the morphology of the laser traces and the cross section of the melt pool were examined. After the evaluation, it was determined that the scanning speed parameters of 600, 800 and 1000 mm/s at a 100 W laser beam power with a

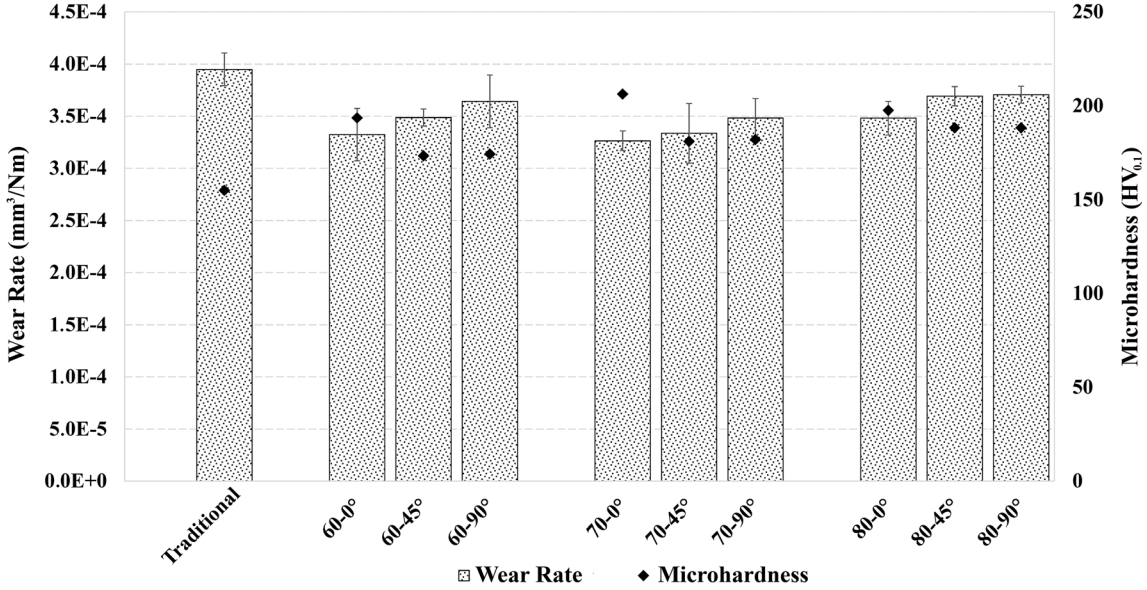

Fig. 14 Microhardness and wear rate graph of the samples manufactured by the traditional method and manufactured by the SLM method using different production parameters

conductive mode and an aspect ratio approaching to 1 provided the optimum melt pool form.

- Contour geometries were produced to examine the molten pool form. After the evaluation, it was determined that the contour wall was quite homogeneous in the productions carried out with a scanning speed of 600 mm/s. According to these examinations, the laser beam power was determined as 100 W and the laser scanning speed was determined as 600 mm/s for a layer thickness of 25 μm.
- According to the wall thickness value determined by the contour geometry production, the amount of hatch spacing value was chosen when it ranged from 30 to 90% with 10% increments. Tensile tests were carried out by producing tensile samples perpendicular to the build platform by using these hatch spacing values. In the study, the elongation value at fracture in terms of mechanical properties was taken as the basis of the performance criterion. After the tensile tests, 60, 70 and 80% hatch spacing values were determined as optimum value range.
- Microstructure examinations were carried out on the samples produced using three different build orientations (0°, 45° and 90°) for the optimum hatch spacing values (60-70-80%) determined after the mechanical examinations. A fine cellular/dendritic structure was detected in the microstructure images. It was observed that the cellular microstructure was dominant in the samples produced with 0° build orientation but some grains grew as dendritic and the microstructure was more homogeneous. It was determined that with the increase of the build orientation (45° $\rightarrow$ 90°), the grains were preferentially oriented and the dendritic growth intensified in the microstructure.
- After tribological investigations, it was determined that the COF values obtained for all samples produced with SLM were lower than the traditionally produced sample. The lowest coefficient of friction values were obtained for samples produced with 60-70% hatch spacing values and 0° build orientation. According to the wear rate values, it was observed that the wear rate increased due to the increase in the build orientation within all three hatch spacing values in the samples produced with the SLM method. The lowest wear rate was obtained for the sample (70-0°) produced with 70% hatch spacing and 0° build orientation. This sample also represents the parameter in which the highest microhardness and density ratio was obtained. The wear rate value of the 70-0° sample was obtained as 17% lower than the wear rate of the sample manufactured with the traditional method. It was determined that 60% and 80% of the hatch spacing values exhibited higher wear rate values compared to 70% in the samples produced with 0° build orientation, where lower wear rates were obtained compared to the traditional sample.

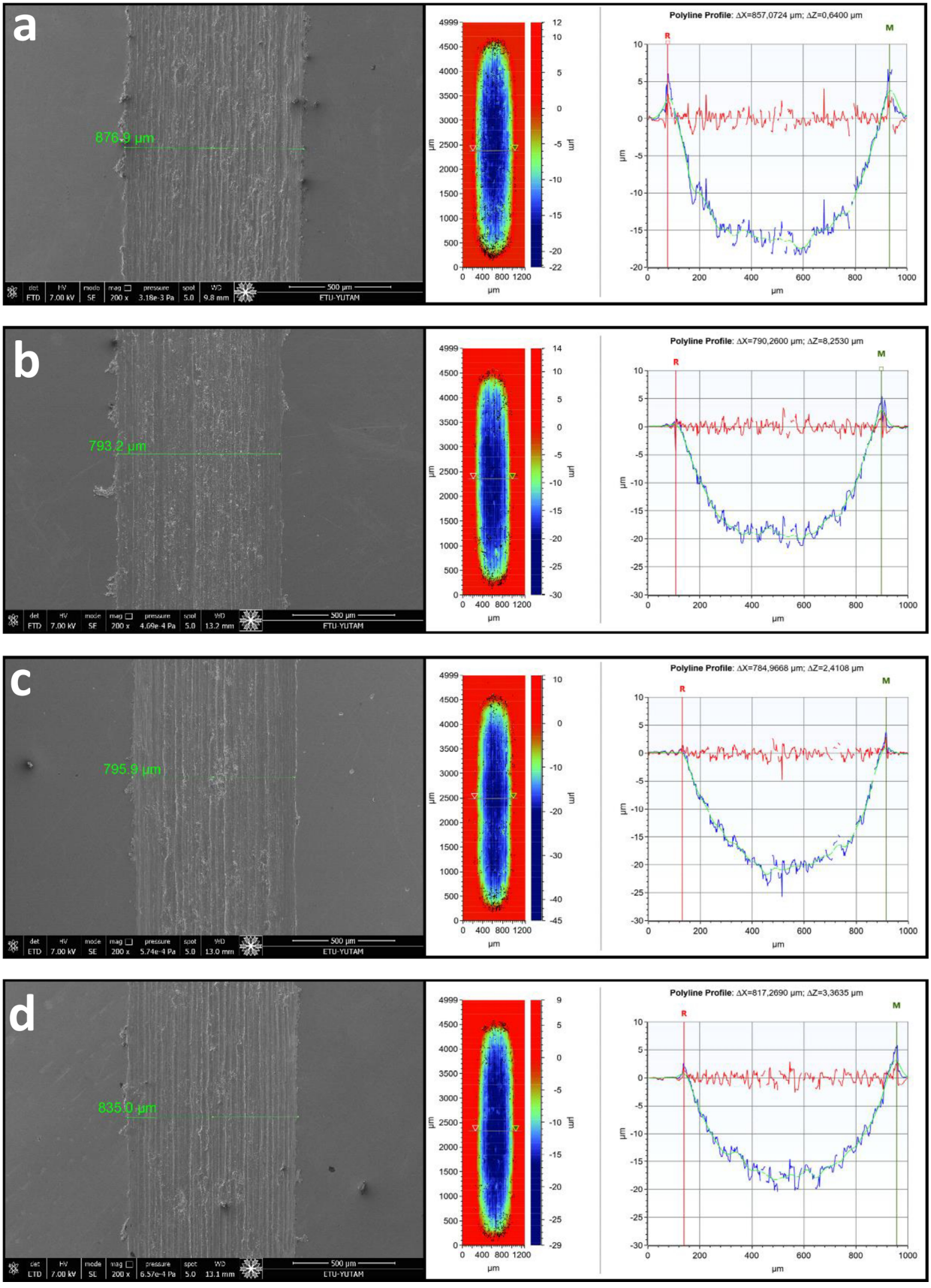

Fig. 15. Wear trace SEM and optical profilometer images of the sample produced with 60% hatch spacing, (a) Traditional sample, (b) 0° build orientation, (c) 45° build orientation, (d) 90° build orientation

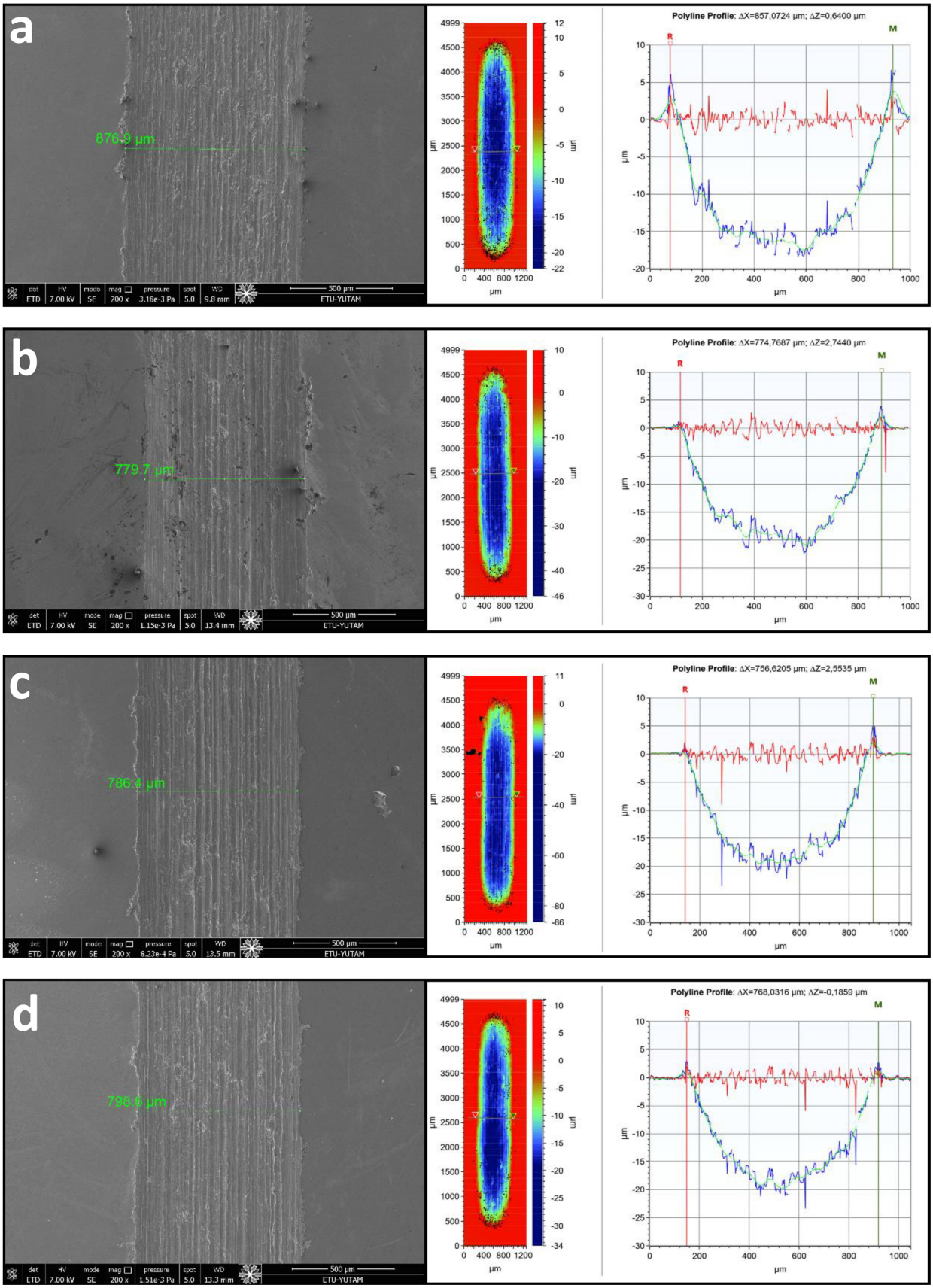

Fig. 16 Wear trace SEM and optical profilometer images of the sample produced with 70% hatch spacing, (a) Traditional sample, (b) 0° build orientation, (c) 45° build orientation, (d) 90° build orientation

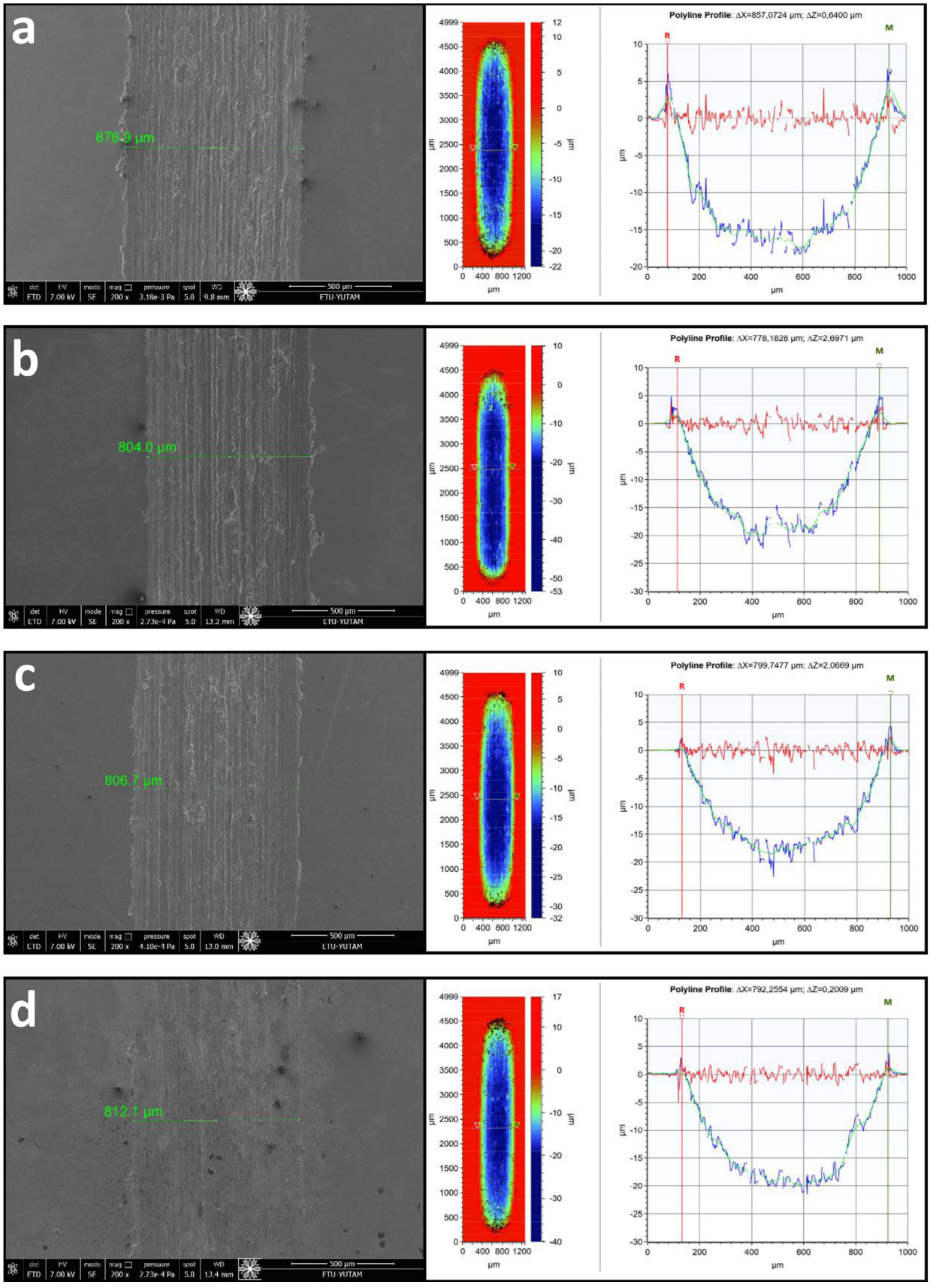

Fig. 17. Wear trace SEM and optical profilometer images of the sample produced with 80% hatch spacing, (a) Traditional sample, (b) 0° build orientation, (c) 45° build orientation, (d) 90° build orientation

Acknowledgments

We would like to thank Erzurum Technical University High Technology Research and Application Center (ETÜ-YÜTAM) for its support in experimental studies. We would also like to thank the Higher Education Council of Turkey (YÖK) for providing scholarships to Tevfik Oğuzhan Ergüder within scope of the 100/2000 program.

Conflict of interest

The authors declare that they have no known competing financial interests or personal relationships that could have appeared to influence the work reported in this paper.

References

1. N. Haghdadi, M. Laleh, M. Moyle and S. Primig, Additive Manufacturing of Steels: A Review of Achievements and Challenges, *J. Mater. Sci.*, 2021, **56**(1), p 64–107.
2. W.M. Tucho, V.H. Lysne, H. Austbø, A. Sjolyst-Kverneland and V. Hansen, Investigation of Effects of Process Parameters on Microstructure and Hardness of SLM Manufactured SS316L, *J. Alloys Compd.*, 2018, **740**, p 910–925.
3. J. Liu, Y. Song, C. Chen, X. Wang, H. Li, C. Zhou, J. Wang, K. Guo and J. Sun, Effect of Scanning Speed on the Microstructure and Mechanical Behavior of 316L Stainless Steel Fabricated by Selective Laser Melting, *Mater. Des.*, 2020, **186**, p 108355.
4. K. Saeidi, X. Gao, Y. Zhong and Z.J. Shen, Hardened Austenite Steel with Columnar Sub-Grain Structure Formed by Laser Melting, *Mater. Sci. Eng. A*, 2015, **625**, p 221–229.
5. H.H. Alsalla, C. Smith and L. Hao, Effect of Build Orientation on the Surface Quality, Microstructure and Mechanical Properties of Selective Laser Melting 316L Stainless Steel, *Rapid Prototyp. J.*, 2018, **24**(1), p 9–17.
6. Y. Zhu, J. Zou, X. Chen and H. Yang, Tribology of Selective Laser Melting Processed Parts: Stainless Steel 316 L under Lubricated Conditions, *Wear*, 2016, **350–351**, p 46–55.
7. W. Shifeng, L. Shuai, W. Qingsong, C. Yan, Z. Sheng and S. Yusheng, Effect of Molten Pool Boundaries on the Mechanical Properties of Selective Laser Melting Parts, *J. Mater. Process. Technol.*, 2014, **214**(11), p 2660–2667.
8. R. Morgan, C.J. Sutcliffe and W. O'Neill, Density Analysis of Direct Metal Laser Re-Melted 316L Stainless Steel Cubic Primitives, *J. Mater. Sci.*, 2004, **39**(4), p 1195–1205.
9. H. Li, M. Ramezani, M. Li, C. Ma and J. Wang, Effect of Process Parameters on Tribological Performance of 316L Stainless Steel Parts Fabricated by Selective Laser Melting, *Manuf. Lett.*, 2018, **16**, p 36–39.
10. Y. Sun, A. Moroz and K. Alrbaey, Sliding Wear Characteristics and Corrosion Behaviour of Selective Laser Melted 316L Stainless Steel, *J. Mater. Eng. Perform.*, 2014, **23**(2), p 518–526.
11. H. Li, M. Ramezani, M. Li, C. Ma and J. Wang, Tribological Performance of Selective Laser Melted 316L Stainless Steel, *Tribol. Int.*, 2018, **128**, p 121–129.
12. Y. Huang, S. Yang, J. Gu, Q. Xiong, C. Duan, X. Meng and Y. Fang, Microstructure and Wear Properties of Selective Laser Melting 316L, *Mater. Chem. Phys.*, 2020, **254**, p 123487.
13. F. Bartolomeu, M. Buciumeanu, E. Pinto, N. Alves, O. Carvalho, F.S. Silva and G. Miranda, 316L Stainless Steel Mechanical and Tribological Behavior—A Comparison between Selective Laser Melting, Hot Pressing and Conventional Casting, *Addit. Manuf.*, 2017, **16**, p 81–89.
14. S. Mohd Yusuf, D. Lim, Y. Chen, S. Yang and N. Gao, Tribological Behaviour of 316L Stainless Steel Additively Manufactured by Laser Powder Bed Fusion and Processed via High-Pressure Torsion, *J. Mater. Process. Technol.*, 2021, **290**, p 116985.
15. Z. Hu, B. Nagarajan, X. Song, R. Huang, W. Zhai and J. Wei, Formation of SS316L Single Tracks in Micro Selective Laser Melting: Surface, Geometry, and Defects, *Adv. Mater. Sci. Eng.*, 2019, **2019**, p 9451406.
16. K. Wei, Z. Wang and X. Zeng, Preliminary Investigation on Selective Laser Melting of Ti-5Al-2.5Sn α-Ti Alloy: From Single Tracks to Bulk 3D Components, *J. Mater. Process. Technol.*, 2017, **244**, p 73–85.
17. Y. Liu, M. Zhang, W. Shi, Y. Ma and J. Yang, Study on Performance Optimization of 316L Stainless Steel Parts by High-Efficiency Selective Laser Melting, *Opt. Laser Technol.*, 2021, **138**, p 106872.
18. Y. Hong, C. Zhou, Y. Zheng, L. Zhang, J. Zheng, X. Chen and B. An, Formation of Strain-Induced Martensite in Selective Laser Melting Austenitic Stainless Steel, *Mater. Sci. Eng. A*, 2019, **740–741**, p 420–426.
19. N.T. Aboulkhair, M. Simonelli, L. Parry, I. Ashcroft, C. Tuck and R. Hague, 3D Printing of Aluminium Alloys: Additive Manufacturing of Aluminium Alloys Using Selective Laser Melting, *Prog. Mater. Sci.*, 2019, **106**, p 100578.
20. S. Enser, H. Yavas, B.A. Hamat, H. Aydın, G. Kafadar, A.A. Tanrıkulu, H.Z. Kazdal, F. Ozturk and M. Güden, Comparing Compression Deformation and Rate Sensitivity of Additively Manufactured and Extruded-Annealed 316L Alloys, *J. Mater. Eng. Perform.*, 2021 https://doi.org/10.1007/s11665-021-06340-9
21. E. Yasa and J.P. Kruth, Microstructural Investigation of Selective Laser Melting 316L Stainless Steel Parts Exposed to Laser Re-Melting, *Procedia Eng.*, 2011, **19**, p 389–395.
22. O.O. Salman, C. Gammer, J. Eckert, M.Z. Salih, E.H. Abdulsalam, K.G. Prashanth and S. Scudino, Selective Laser Melting of 316L Stainless Steel: Influence of TiB_2 Addition on Microstructure and Mechanical Properties, *Mater. Today Commun.*, 2019, **21**, p 100615.
23. Z. Sun, X. Tan, S.B. Tor and W.Y. Yeong, Selective Laser Melting of Stainless Steel 316L with Low Porosity and High Build Rates, *Mater. Des.*, 2016, **104**, p 197–204.
24. D. Wang, C. Song, Y. Yang and Y. Bai, Investigation of Crystal Growth Mechanism during Selective Laser Melting and Mechanical Property Characterization of 316L Stainless Steel Parts, *Mater. Des.*, 2016, **100**, p 291–299.
25. V. Kumar, M.D. Joshi, C. Pruncu, I. Singh and S.S. Hosmani, Microstructure and Tribological Response of Selective Laser Melted AISI 316L Stainless Steel: The Role of Severe Surface Deformation, *J. Mater. Eng. Perform.*, 2021, **30**(7), p 5170–5183.
26. A.F. Yetim, F. Yildiz, A. Alsaran and A. Çelik, Surface Modification of 316L Stainless Steel with Plasma Nitriding, *Kov. Mater.*, 2008, **46**(2), p 105–116.

Publisher's Note Springer Nature remains neutral with regard to jurisdictional claims in published maps and institutional affiliations.